The Effect of Droplets in the Air-Sea Transition Zone on the Sea Brightness Temperature

C. C. H. TANG [1]

Jet Propulsion Laboratory, California Institute of Technology, Pasadena 91103

(Manuscript received 26 September 1973, in revised form 10 April 1974)

ABSTRACT

A model is presented depicting that, for a fully developed sea driven by the wind with speeds above 5 m sec^{-1}, the air in the transition zone immediately above the air-sea interface is mixed with sea water droplets from bursting air bubbles. The absorptive droplet concentration in the zone is assumed to have a profile tapering off from the interface to zero at a certain height. The dielectric constant of the absorptive inhomogeneous droplet profile is thus both a function of the wind speed and the height above the interface. Both the inhomogeneity effect and the absorption-emission effect of the droplet concentration have been considered.

Theoretical calculations show that the presence of the absorptive inhomogeneous droplet transition zone significantly increases the sea brightness temperature as wind speed rises. Combined effects of both the droplet areas and the foam areas on sea surface also have been considered.

A brief review and discussion of related recent investigations is included.

1. Introduction

In the last few years considerable efforts have been made both theoretically and experimentally in studying the characteristics of microwave emission from a wind-driven sea. The first extensive measurement of the brightness temperature of a sea was made in 1968 at 19.35 GHz by Nordberg *et al.* (1969) with a Convair-990 jet aircraft. Their observed results are reproduced in Fig. 1 which also shows the results of the theoretical model developed by Stogryn (1967). In his model, he made use of the sea slope measurements by Cox and Munk (1954) who related the density of the reflected images of the sun to the statistics of the wave slopes and found that the slope distributions were nearly Gaussian. From Fig. 1 we note that over the calm sea there is general agreement between observation and theory if a vertical scale shift is allowed. In contrast, there is apparent disagreement between observations and Stogryn's theoretical results at 14 m sec^{-1} wind speed. The observed results for this wind speed show at all nadir angles an almost uniform increase of temperature over those for the case of a calm sea; the theoretical analysis, however, does not indicate such an increase in the temperature at nadir. It has been speculated that the discrepancy at high wind speeds might be due to the effect of sea foam which has not been taken into account in Stogryn's analysis. Nordberg *et al.* (1971) made further extensive measurements of microwave emission at 19.35 GHz from the North Atlantic Ocean surface in 1969. Their observation results are reproduced in Table 1 and Fig. 2; they estimated from Fig. 2 that the measured difference between the results of the two wind speeds is at least 22C (after corrections for sky temperature and atmospheric emission) at all nadir angles. In addition, they established from their results (after corrections for sky temperature and atmospheric emission) that for wind speeds exceeding 5 or 6 m sec^{-1} the brightness temperature at nadir increases almost linearly with increasing wind speed at a rate of 1.2C $(m\ sec^{-1})^{-1}$. Although these two groups of observations certainly contain some measurement inaccuracy, it appears that these data clearly establish the fact that at nadir the brightness temperature increases with increasing wind speed. On the other hand, the theoretical analysis of Stogryn does not predict such a trend.

In view of the discrepancy between the theoretical model and the observations, a brief comparison of available theoretical models and their corresponding results is in order. A search of the Russian literature reveals that Shifrin and Ionina (1968) made a theoretical analysis on the same subject also using the sea slope measurements by Cox and Munk (1954) as did Stogryn. Neither model considered the effect of foam formation. Shifrin explicitly expressed the angle between the incident beam and the local normal $\hat{n}$ to the sea area selected for observation in terms

[1] Work performed under NASA Contract NASW-417.

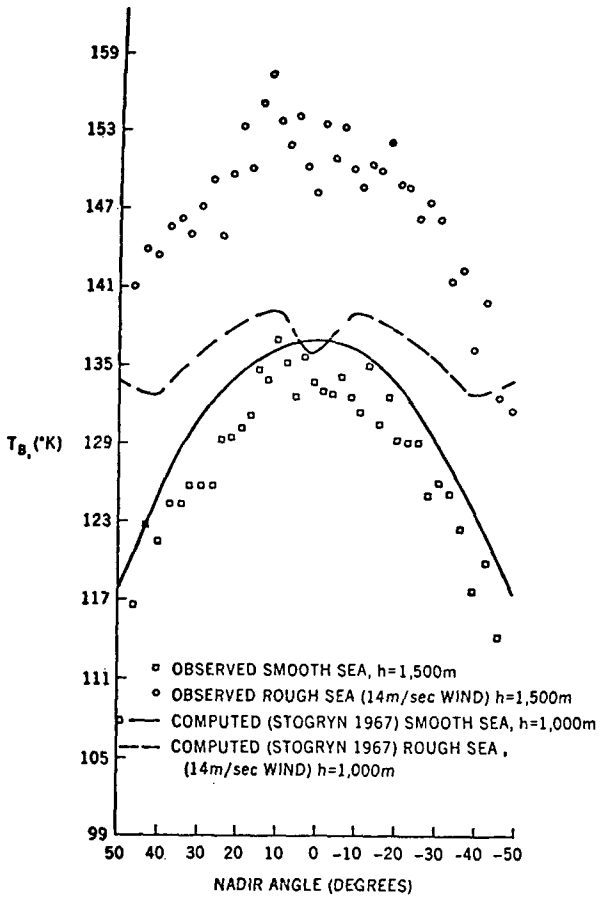

FIG. 1. Observed and computed (Stogryn, 1967) brightness temperatures vs nadir angle at 1.55 cm over smooth and rough portions of the Salton Sea. Computations are for a sea surface temperature of 290K and a standard atmosphere. Observations were made with a sea surface temperature of 294K over a rough sea and 300K over a smooth sea in a relatively moist atmosphere on 7 June 1968. Each point shown for the observed data represents an average of six consecutive scans at the respective nadir angle.

of the angle between the direction of observation and the normal $\hat{z}$ to the horizon. Shifrin and Ionina assumed that all wind directions are equally probable whereas Stogryn assumed that the crosswind case is different from the upwind case. They also used differential scattering coefficients in different forms. Shifrin used the method of steepest descent whereas Storgyn used numerical integration procedures. Due to these differences in theoretical modeling, their results also appear somewhat different as shown in Figs. 3 and 4 for three typical wind speeds. We note that for horizontal (or vertical) polarization at large nadir angles the emissivity of Stogryn's model rises (or drops) much faster at high wind speeds than that of Shifrin's. For vertical polarization at nadir, the two models show opposite predictions. On the other hand, neither model predicts that emissivities increase with increasing wind speed at nadir. In the following section, we shall present a modified theoretical approach that models more accurately the actual physical environment in the transition zone immediately above the air-sea interface than the presently available theoretical models do.

2. Modified theoretical model

The brightness temperature T_B measured by an aircraft or spacecraft at height H can be expressed as

$$T_B=[ET+(1-E)T_s]\tau(H)+\int_0^H T_A(h)\frac{\partial\tau(h)}{\partial h}dh, \quad (1)$$

where E is the emissivity of the sea surface, T the surface temperature of the sea, T_s the sky brightness temperature at the sea surface, T_A the temperature of the atmosphere, and τ the transmissivity of the atmosphere which can be expressed as

$$\tau=\exp\left[-\sec\theta_1\int_0^h k\rho dh\right], \quad (2)$$

where ρ is the density of absorbing gases in the atmosphere, k the absorption coefficient for these gases, and θ_1 a nadir angle of observation. Note that all the terms in (1) are sensitive functions of the density profiles of absorbing gases in the atmosphere at the time of observation. These terms therefore are sources of uncertainty in theoretical computations if the water vapor profile is not known during measurements. Assuming that uncertainties in these terms could be accounted for, we shall restrict the remainder of our study to the theoretical computation of the sea surface emissivity in a model that simulates the actual physical situation.

For a perfectly smooth air-sea interface, the emissivity can be conveniently evaluated as

$$E=1-R, \quad (3)$$

where R is the Fresnel energy reflection coefficient for either horizontal or vertical polarization:

$$R_h=\left|\frac{\cos\theta_1-(\epsilon-\sin^2\theta_1)^{\frac{1}{2}}}{\cos\theta_1+(\epsilon-\sin^2\theta_1)^{\frac{1}{2}}}\right|^2, \quad (4)$$

$$R_v=\left|\frac{\epsilon\cos\theta_1-(\epsilon-\sin^2\theta_1)^{\frac{1}{2}}}{\epsilon\cos\theta_1+(\epsilon-\sin^2\theta_1)^{\frac{1}{2}}}\right|^2, \quad (5)$$

where ϵ is the complex dielectric constant of sea water. We emphasize here that θ_1 is a nadir angle, i.e., the angle between the direction of observation and the normal to the perfectly smooth, horizontally inclined water surface.

The wavy rough sea surface is assumed to consist of a set of smooth areas, the normals to which have a Gaussian distribution described by Cox and Munk (1954). The diffraction at the edges of an area is

TABLE I

SUMMARY OF METEOROLOGICAL CONDITIONS AND MICROWAVE EMISSION TEMPERATURES FOR SIX OVERWATER FLIGHTS

	Case					
	A	B	C	D	E	F
Date (March 69)	10	13	13	10	19	14
Time (GMT)	1321	1247	1117	1430	1023	1453
Location	Atlantic Off Shannon	Atlantic Ship J	Atlantic Ship I	Atlantic Ship I	North Sea 57°N 3°E	North Sea 59°N 1°30′E
Wind speed (m sec^{-1})	<5	6	13	16	17	25
Significant wave height (m)	<1	6.0†	3.9	5.0	4.0	7.8
Foam cover (%)						
Whitecaps	—	—	4.2	5.6	6.0	5.0
Streaks	—	—	3.5	6.9	17.4	27.0
Total	—	—	7.7	12.5	23.4	32.0
Temperature (°C)						
Sea surface	9	10	9	9	2	4
Air surface	10 (est.)	11	7	5	2	2
Cloud altitude (m)						
Base	2000	clear	300	800	600	150
Top	2300	clear	2100	2000	2000	5000
Brightness temperature (°K)						
High altitude*	128**	—	—	138	138	148
Low altitude	120	118	127	132	132	142

* Measured within 30 min of time shown.
** Over Irish Sea at 1212 GMT.
† All swell, no wind waves.

neglected by using the geometric optics approximation. Fig. 5 shows that the true or local angle of incidence between $\hat{n}$ and the incident beam is χ. According to the Fresnel formulas, the angle χ should be used in Eqs. (4) and (5) for a wavy sea surface instead of the angle θ_1. We shall adopt the Shifrin approach in view of its compact computational form. Shifrin has shown that

$$E=1-\sec\theta_1\int P[\theta_n(v),\phi_n(v)] \times\cos\chi\,\sec^4\theta_n R(\chi)\,\sin\theta_n d\theta_n d\phi_n,$$

$$=1-0.502\left[\left(1+\sqrt{\frac{C}{2}}\tan\theta_1\right)R(\chi^+) +\left(1-\sqrt{\frac{C}{2}}\tan\theta_1\right)R(\chi^-)\right], \quad (6)$$

where $P[\theta_n(v), \phi_n(v)]$ is the Cox and Munk distribution function with coefficients that depend on the wind speed, and

$$C=0.0015+0.00254v, \quad (7)$$

$$\chi^+=\cos^{-1}\left[\frac{1}{(1+C)^{\frac{1}{2}}}\left(\cos\theta_1+\sqrt{\frac{C}{2}}\sin\theta_1\right)\right], \quad (8)$$

$$\chi^-=\cos^{-1}\left[\frac{1}{(1+C)^{\frac{1}{2}}}\left(\cos\theta_1-\sqrt{\frac{C}{2}}\sin\theta_1\right)\right]. \quad (9)$$

Note that $\chi^+=\chi^-=\theta_1$ when C vanishes. We also mention that (i) Eq. (6) is not to be used for $v>30$ m sec^{-1}, since the Cox-Munk distribution is probably no longer valid for $v>30$ m sec^{-1}, and (ii) Eq. (6) has an error of about 1% as a result of using the steepest descent integration method. For $\epsilon=35.62-i37.05$, which is the value used by Stogryn in Fig. 3, evaluation of Eq. (6) yields the results shown in Fig. 4.

In using Eqs. (4) and (5) both Shifrin and Stogryn implied that the dielectric constant ϵ_0 of the air immediately above the sea is unity, i.e., the effects of foam and other factors can be ignored. In physical reality, it appears that the dielectric constant ϵ_0 of the air immediately above the sea could be a function of both the wind speed v and the height z. Eqs. (4) and (5) should thus take the general forms:

$$R_h=\left|\frac{\cos\chi-\left[\frac{\epsilon}{\epsilon_0(v,z)}-\sin^2\chi\right]^{\frac{1}{2}}}{\cos\chi+\left[\frac{\epsilon}{\epsilon_0(v,z)}-\sin^2\chi\right]^{\frac{1}{2}}}\right|^2, \quad (10)$$

$$R_v=\left|\frac{\frac{\epsilon}{\epsilon_0(v,z)}\cos\chi-\left[\frac{\epsilon}{\epsilon_0(v,z)}-\sin^2\chi\right]^{\frac{1}{2}}}{\frac{\epsilon}{\epsilon_0(v,z)}\cos\chi-\left[\frac{\epsilon}{\epsilon_0(v,z)}-\sin^2\chi\right]^{\frac{1}{2}}}\right|^2. \quad (11)$$

We shall use Eqs. (10) and (11) in Eq. (6) as the basis to develop the modified theoretical model which we hope will simulate the actual physical environ-

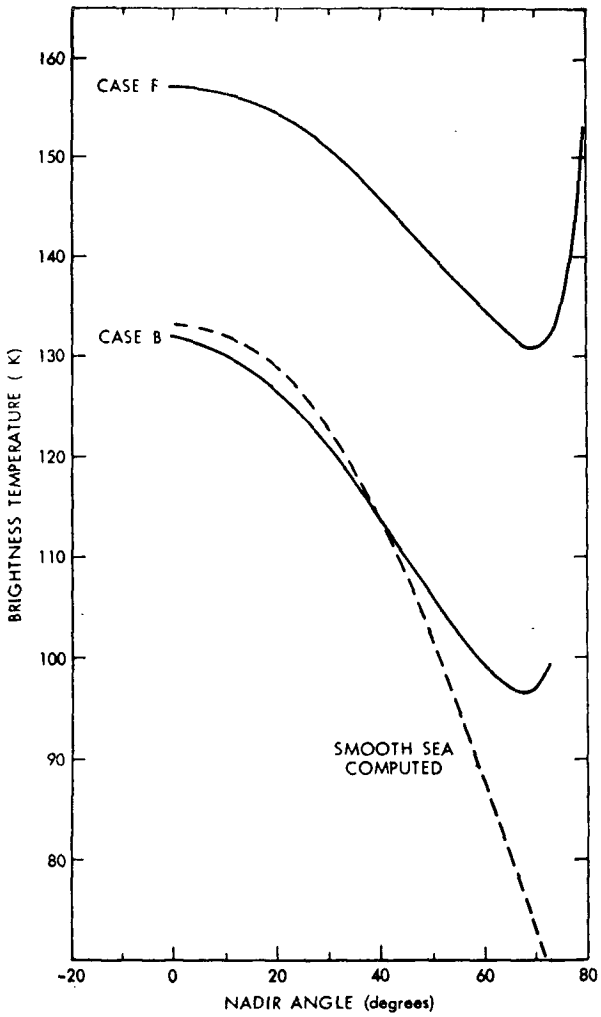

FIG. 2. Brightness temperatures averaged for 10–29 sec time periods, for each antenna scan angle during 30° aircraft banks, vs nadir angle for case B of Table 1 (lower curve) and case F of Table 1 (upper curve). Absolute brightness temperatures were normalized to computations for a smooth sea (dashed curve) at nadir. The dashed curve shows computed brightness temperatures for atmospheric and sea surface temperatures encountered in case B but for a smooth, specular sea surface.

ment in the vicinity of the air-sea interface as closely as possible. The essence of the problem then is to model first the dielectric constant $\epsilon_0(v,0^+)$, i.e., immediately above the interface at $z=0^+$, as a function of the wind speed in a physically plausible manner. This will be done in the next section by utilizing all relevant information obtained from observations of the air-sea interface.

3. Dielectric constant model of the air immediately above the air-sea interface

The physics of the marine atmosphere and of disturbances of the sea surface is not yet well understood. The more or less periodic disturbances of the sea surface generally originate from atmospheric, seismic and astronomical causes and comprise a period range from about 10^{-2} to 10^5 sec (Munk, 1950). The energy is concentrated in the ordinary gravity waves (periods 1 to 30 sec) and in the ordinary tides (periods about 12 to 24 hr). Gravity waves are generated by the wind and mainly governed by gravitational and inertial forces. If the waves are growing or being maintained by the local wind they are called sea, whereas waves that are no longer under the action of the generating wind are termed swell. The frictional coupling between wind and sea surface is a very intricate problem. Superimposed on the big gravity waves are capillary waves (small wavelets and ripples of less than 2 cm in length) generally controlled by forces associated with surface tension. Evidence is growing that these tiny ripples represent the drag of the wind on the sea much more than the big waves do. Gravity waves are normally dispersive, whereas capillary waves show anomalous dispersion.

In searching for a realistic model of the transitional zone above the air-sea interface, we shall use some of the observed results that led to a partial explanation of the mechanism of sea-salt nuclei production in the atmosphere. It is known that when the wind over the sea is strong enough to create whitecaps, air is trapped by the collapsing wavecrests and rises to the sea surface in the form of small air bubbles or foam. In addition, all forms of precipitation particles are effective bubble producers when striking the sea surface as shown by Blanchard and Woodcock (1957). These air bubbles, when bursting at the sea surface, cause a transport of sea water droplets into the air via two processes: the bubble film droplets and the bubble jet droplets. The droplets thus formed create a transition zone at the air-sea interface. The bubble film droplets originate from the disintegration of the bubble film, that section of the bubble that protrudes through the air-sea interface. The hemispherical film cap of a bubble rising from below breaks the surface where it is thinnest, causing a disintegration of the bubble film into hundreds of fine droplets. The bubble jet droplets emerge, after the bursting of the film cap, from a narrow unstable jet evolving from the bottom of the collapsing bubble and then breaking into a few large droplets. Fig. 6 is a reproduction from Blanchard's paper (1963) showing consecutive stages of the bursting of an air bubble into jet droplets. Blanchard's experiments give the following information. The bubble diameter varies from less than a millimeter up to a centimeter and the corresponding bubble film area varied from less than 10^{-4} cm^2 up to 1 cm^2. The diameter of jet droplets has a range from a few micrometers up to a millimeter or so. The jet droplets could be ejected at speeds as large as 10^4 cm sec^{-1}, and rise as high as 15 cm. The magnitude of the jet droplet production appears to be proportional to the

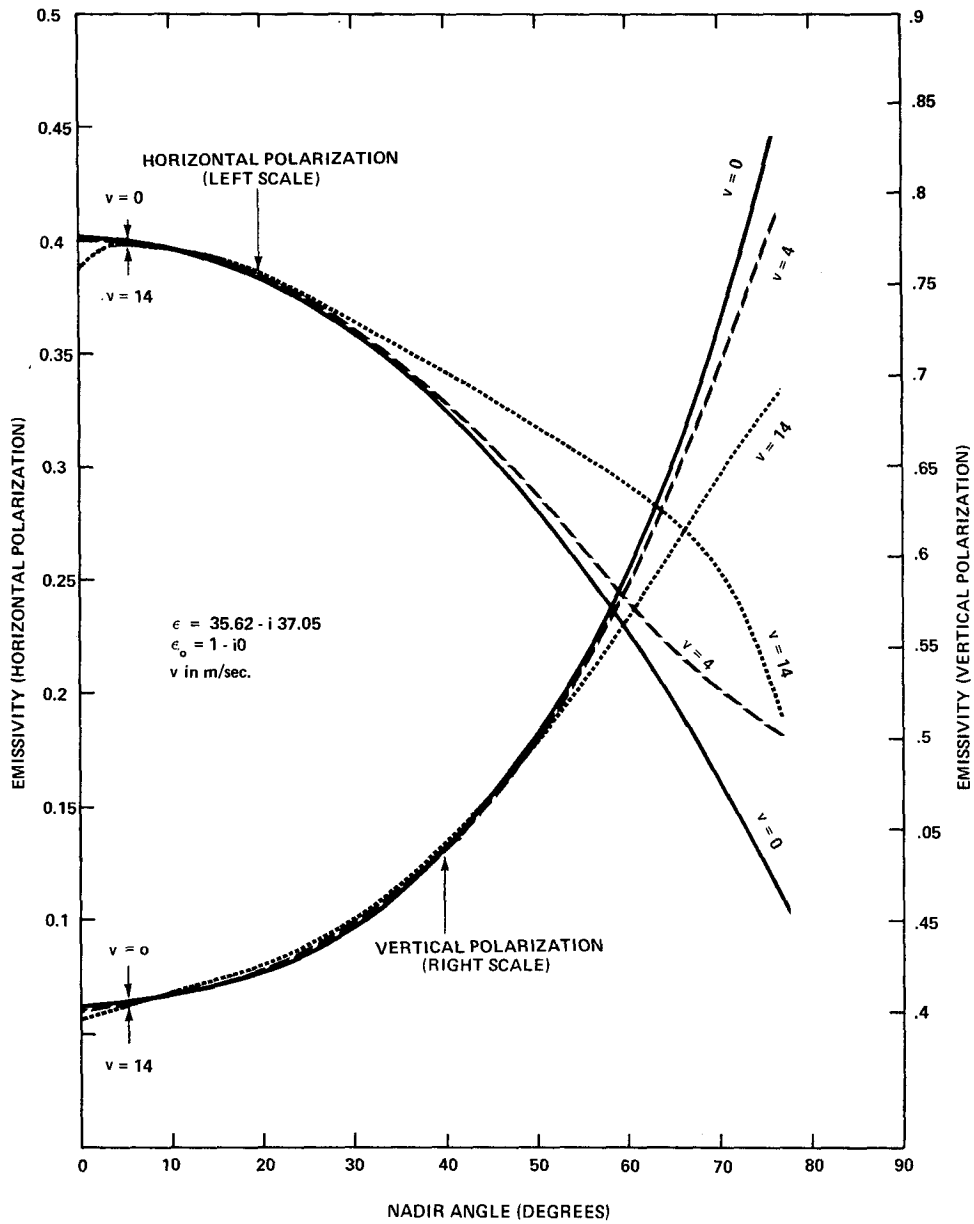

FIG. 3. Emissivity curves according to Stogryn.

wind speed in the range from 5 m sec^{-1} ($\sim$0.02 droplet cm^{-2} sec^{-1}) to 15 m sec^{-1} ($\sim$0.1 droplet cm^{-2} sec^{-1}). The bubble film droplets have diameters varying from 5 to about 20 μm and can travel up to more than 1 cm. The number of film droplets produced is proportional to the diameter of the film cap. A 2-mm diameter bubble (film cap area about 0.005 cm^2) will produce a maximum of about 100 film droplets and a 6-mm diameter bubble (film cap area about 0.3 cm^2) a maximum of 1000 film droplets. Blanchard also showed that the percent of ocean covered with whitecaps is approximately proportional to the square of the wind speed.

It appears from the information described in the above paragraph that for a fully developed sea (i.e., wind-driven sea in a steady state) a majority of the bubbles from patches of whitecaps will spread and distribute over the sea. The bursting of these bubbles will mix the air immediately above the interface with sufficient sea water droplets to make the dielectric constant of the mixture larger than unity. It is plausible to assume that in the transition zone the concentration of these sea water droplets will taper off from the interface to zero at a certain height according to some kind of profile. The effect of the inhomogeneous droplet concentration profile on the trans-

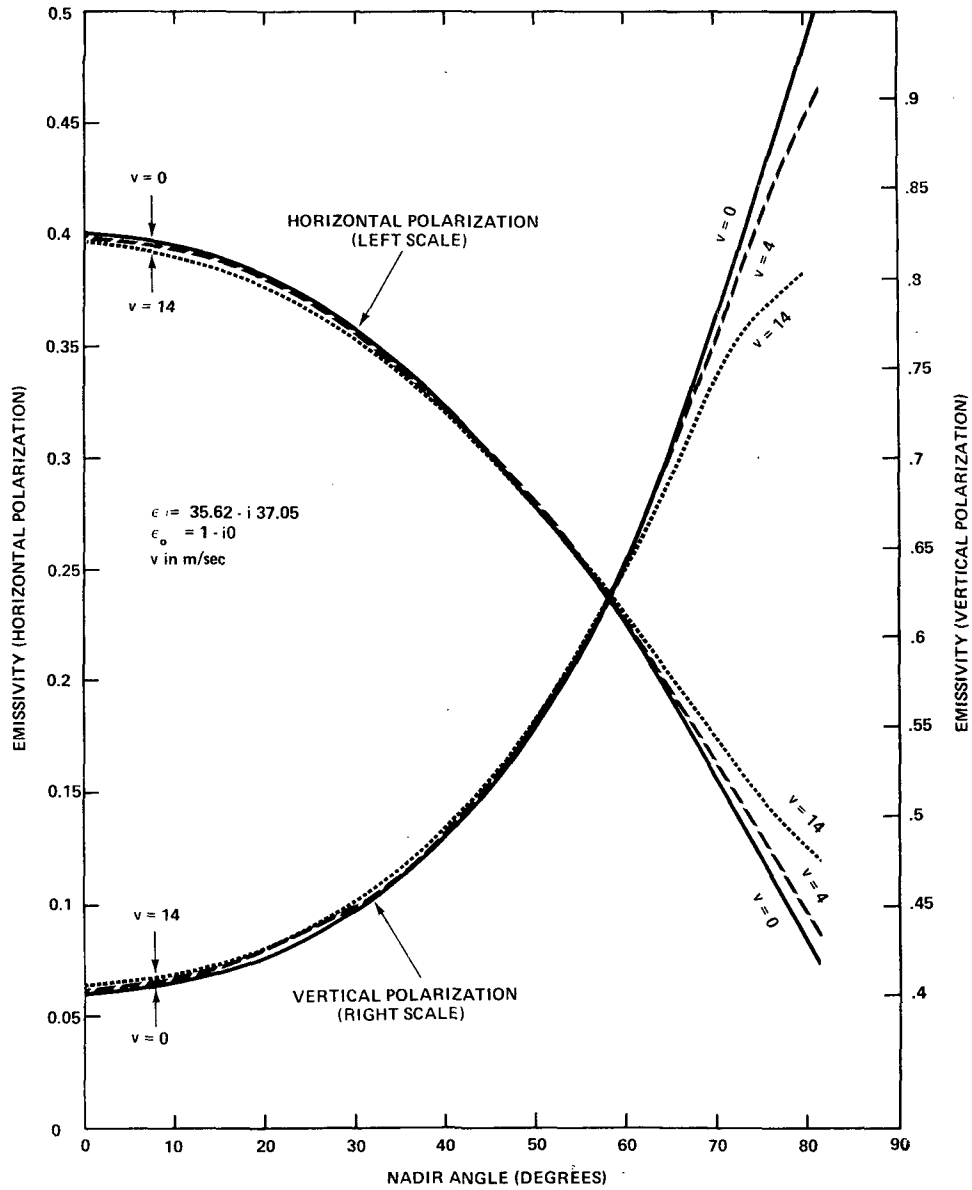

FIG. 4. Emissivity curves according to Shifrin.

mission of the thermal emission from the sea surface will be studied later. We shall first simulate the variation of the dielectric constant of the interface air mixed with sea water droplets, the concentration of which is a function of both the wind speed and the height from the interface. Immediately above the interface, a simple linear model has the form

$$\epsilon_0(v,0^+)=1+(\epsilon-1)p, \tag{12}$$

where p is the percent of sea water droplets in the air immediately above the interface. Note that $\epsilon_0(v,0^+)$ is unity for $p=0$ and is equal to ϵ for $p=1$. We now assume that p varies as a function of the wind speed v, i.e.,

$$p=C_1+C_2v+C_3v^2. \tag{13}$$

The constant term C_1 takes care of the facts (i) that measurements by Nordberg *et al.* (1971) show almost no brightness temperature change for winds from calm to about 5 m sec^{-1}; and (ii) that the transition from a smooth sea to a sea beginning to form scattered whitecaps seems to occur at wind speeds between 5 and 7 m sec^{-1} [Munk (1947) and Mandelbaum (1956) concluded that at such wind speed the sea surface undergoes an abrupt discontinuity involving the transition from laminar to turbulent flow]. The linear term C_2v is consistent with the observation that the

droplet production rate appears to be proportional to the wind speed at low range (5–15 m sec^{-1}), and the C_3v^2 term indicates that the percent of whitecap coverage is approximately proportional to the square of the wind speed.

The constant C_1 can be determined in terms of C_2 and C_3 for a particular choice of v at which the whitecaps begin to appear. This speed could be any value between 5 and 7 m sec^{-1} as mentioned earlier and we arbitrarily choose $v=5$ m sec^{-1} for convenience in computation. This number also appears to be reasonable according to Roll's (1965) wind force chart. The chart indicates that at wind speeds between 4.5 and 6.6 m sec^{-1}, the sea surface has large wavelets and begins to form breaking crests and foam and perhaps scattered whitecaps. By setting $p=0$ and $v=5$ in Eq. (13), we have

$$C_1=5C_2-25C_3, \tag{14}$$

$$\epsilon_0(v,0^+)=\begin{cases}1+(\epsilon-1)[(v-5)C_2+(v^2-25)C_3], & \\ \qquad\qquad\qquad\qquad \text{for} \quad v\geqslant 5 \\ 1, \qquad\qquad\qquad\qquad \text{for} \quad v\leqslant 5.\end{cases} \tag{15}$$

Our objective now is to determine the constants C_2 and C_3, if possible, such that $\epsilon_0(v,0^+)$ will vary with the wind speed in a manner satisfying the observed fact that at nadir the brightness temperature for the horizontal polarization increases with increasing wind speed at some measured rate.

Since $\epsilon_0(v,0^+)$ is a function of the sea water dielectric constant ϵ, we must first determine ϵ as accurately as possible. It is well known that the dielectric constant of the sea water is a sensitive function of the emission wavelength, salinity and temperature. An accurate evaluation of ϵ that represents experimental values well was not available until recently. Fig. 7 shows the complex dielectric constant of sea water for an average salinity of 36‰ in the North Atlantic Sea and a temperature of 7C, which is obtained by roughly averaging sea surface temperatures for the cases shown in Table 1. At 19.35 GHz (1.55 cm), $\epsilon=23.41-i33.63$ from Fig. 7.

With the given complex value of ϵ and the use of Eqs. (15), (10) and (6) we see that the complex $\epsilon_0(v,0^+)$ as a function of increasing wind speed can be derived by suitably choosing the values of C_2 and C_3 such that the calculated brightness temperatures (for the horizontal polarization at nadir) for increasing wind speeds are in general agreement with the corresponding observed brightness temperatures. Before actually carrying out the computation, we shall in-

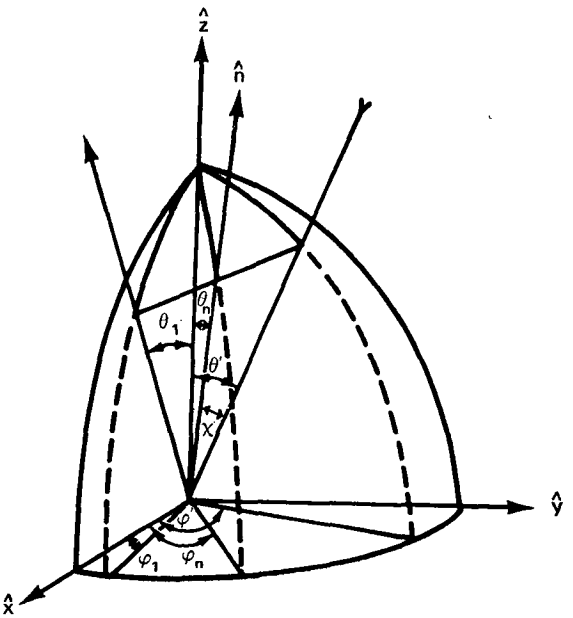

θ_1 and φ_1 are respectively the nadir angle and the azimuthal angle of the observation point.
θ' and φ' are respectively the nadir angle and the azimuthal angle of the incident beam.
θ_n and φ_n are respectively the nadir angle and the azimuthal angle of the local normal to the selected area to be observed on the surface of the sea.
χ is the true or local angle of incidence

FIG. 5. Scattering geometry.

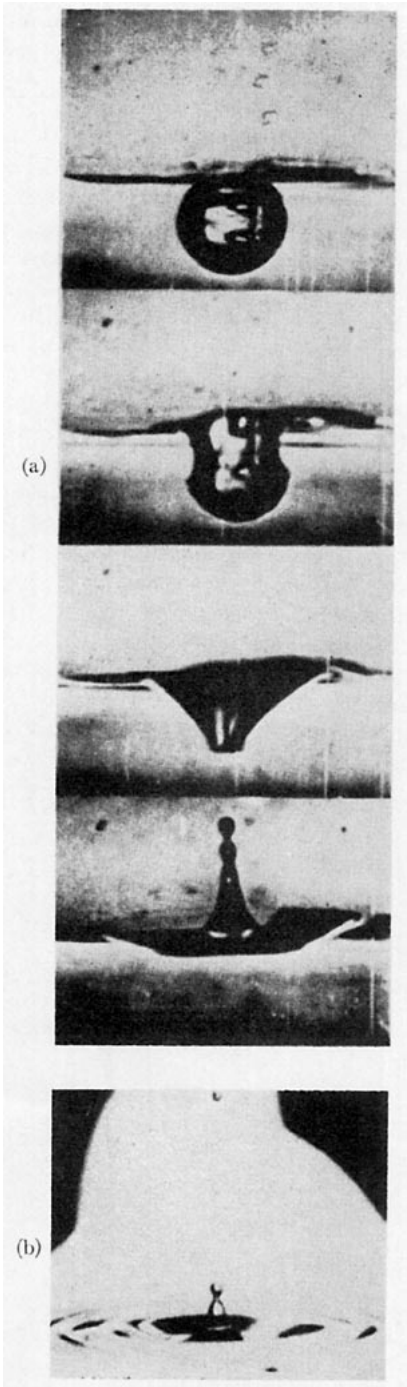

FIG. 6. (a) Composite view of high-speed pictures illustrating some of the stages in the collapse of a 1.7-mm diameter bubble. The time interval between top and bottom frames is about 2.3 msec. The angle of view is horizontal through a glass wall. The surface irregularities are due to a meniscus. (b) Oblique view of the jet from a 1-mm diameter bubble.

vestigate 1) the effect of an air-sea transition zone (of depth h) with an inhomogeneous complex dielectric constant profile $\epsilon_0(v,z)$ having boundary conditions $\epsilon_0(v,0)=\epsilon$ and $\epsilon_0(v,h)=1$; and 2) the components of the measured brightness temperature due to the presence of such an absorptive transition zone.

4. Effects of an inhomogeneous droplet profile on brightness temperature

It was mentioned in Section 3 that the sea water droplet concentration profile could affect the transmission of microwave emission from the sea surface. To study this problem we have to find the transmissivity of electromagnetic waves in a lossy inhomogeneous finite medium at an oblique incidence. Analytic results of this general problem do not appear to be available, but approximate results of lossless inhomogeneous finite media at normal incidence have recently been obtained (Tang, 1974). We shall use those results to get a general idea of the nature of the problem in the nadir direction. To do this we must first assume the form of the droplet concentration profile F in terms of the parameter ρ_h, i.e.,

$$\rho_h=\int_0^h \frac{2\pi}{\lambda}[\epsilon_0(v,z)]^{\frac{1}{2}}dz, \tag{16}$$

where λ is the free-space wavelength of the microwave emission, and h the height at which $\epsilon_0(v,h)$ is equal to unity, i.e., above h the droplets no longer contribute to the value of dielectric constant due to their sparse distribution, if any. For a profile with droplet concentration (or sea water content) decreasing with height and having at least its first derivative vanishing at $z=h$, we assume the profile F has the form

$$F=\left[\cos\left(\frac{\pi}{2}\frac{\rho}{\rho_h}\right)\right]^J, \quad J=2, 3, 4, \cdots, \tag{17}$$

where

$$\rho=\int_0^z \frac{2\pi}{\lambda}[\epsilon_0(v,z)]^{\frac{1}{2}}dz, \tag{18}$$

with z varying from 0 to h, i.e., ρ varying from 0 to ρ_h.

The dielectric constant $\epsilon_0(v,z)$ of the transition zone between $z=0^+$ and $z=h$ can then be expressed in the general form

$$\epsilon_0(v,z)=1+AF=1+A\left[\cos\left(\frac{\pi}{2}\frac{\rho}{\rho_h}\right)\right]^J, \tag{19}$$

where

$$A=\epsilon_0(v,0^+)-1. \tag{20}$$

Since Tang's results (1974) are for the lossless case only, we use only the real part of the sea water dielectric constant ϵ_0 in actual computations. The computational results of the transmissivity (for normal incidence) of inhomogeneous lossless sea water droplet profiles are shown in Fig. 8 for cases with $J=2$ and 5 and several assumed values of the parameter A. The pips in the figure indicate the transmissivities of the profiles when the ratio (h/λ) of the profile height h to the wavelength λ of the emission is a half-wavelength.

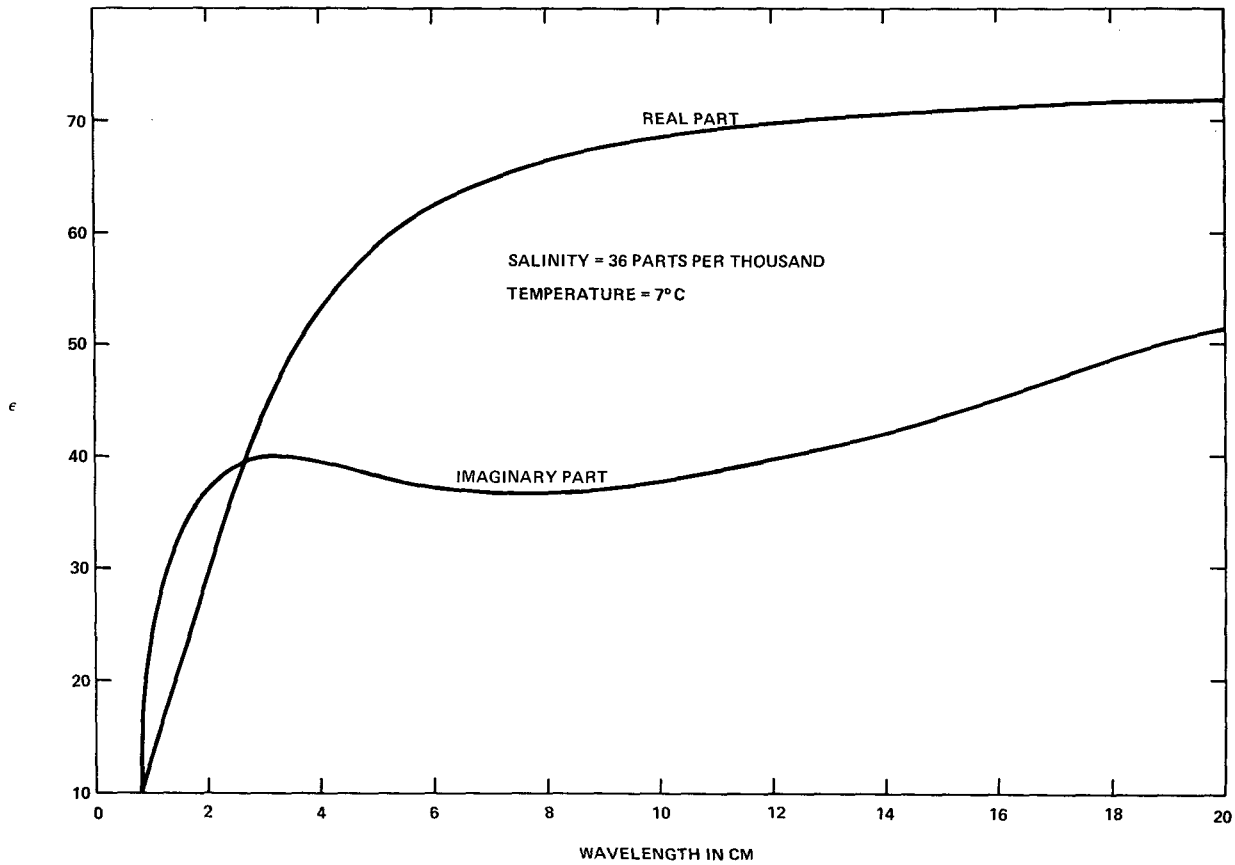

FIG. 7. Complex dielectric constant ϵ of sea water.

It is evident from Fig. 8 that for most cases the transmissivity is practically unity when h is larger than $\frac{3}{4}\lambda$. For cases with $A<0.3$ the transmissivity is almost unity for $h>\frac{1}{2}\lambda$. The height h most likely will increase somewhat with increasing wind speed. Accordingly, we may speculate that even at high wind speeds when $\epsilon_0(v,z)$ is relatively large, the transmissivity is close to unity for emissions with λ of the order of a few centimeters. In Section 3 we mentioned that a bubble film could burst into hundreds of fine droplets at a height up to 1–2 cm and a bubble jet could eject a few large droplets at a height up to 10–15 cm. It appears that the droplet concentration is highest within the first few centimeters for a fully developed sea. Thus, for microwave emissions of wavelengths comparable to the depth of the transition zone the reflectivity of the zone could be vanishingly small. At wavelengths much longer than the zone depth the reflectivity might rise and the problem becomes rather complicated due to relatively large number of multiple reflections within the transition zone.

Although what has been said in the above paragraph is derived from computations for lossless cases, the general trend should also hold for lossy cases; i.e., the resultant reflection due to an inhomogeneous and lossy transition zone of dielectric constant profile shown in Eq. (17) is in general negligible if the zone depth is of the order of a wavelength or more. With this understanding of negligible resultant reflection from the inhomogeneous lossy transition zone, we are now in a position to estimate the theoretical apparent brightness temperatures of the air-sea interface in the presence of an inhomogeneous lossy transition zone. Assuming the effective emissivity of the interface between the sea and the transition zone (depth of the order of a wavelength) is E, the thermometric temperature of sea and the air immediately above is T, and the transmissivity due to the presence of absorption in the transition zone of depth h is τ_h, we note that the apparent radiation emitting from the sea is $ET\tau_h$. The radiation originating from the transition zone has two parts, one upward and one downward, the latter being reflected at the interface between the sea and the transition zone and then attenuated by the transition zone. The upward radiation of the attenuating zone is

$$\int_0^h T\frac{\delta\tau_h}{\delta z}dz = T(1-\tau_h)$$

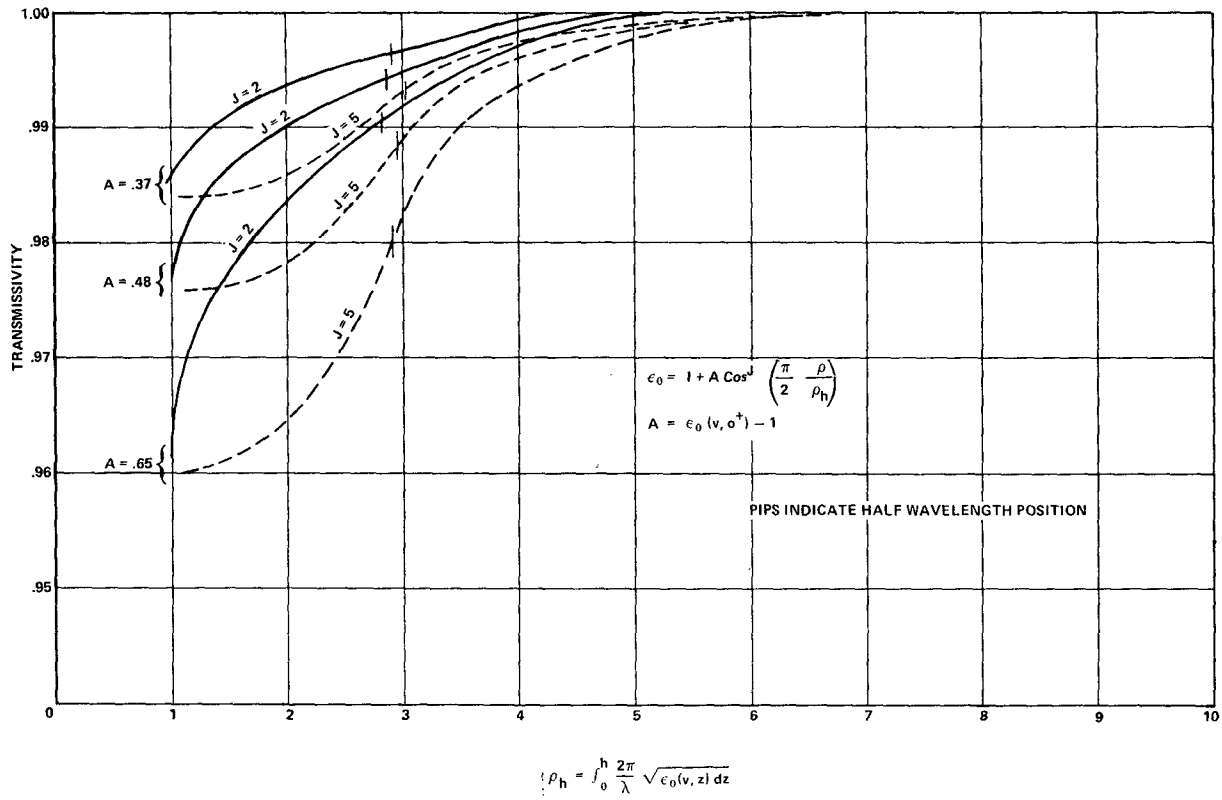

FIG. 8. Transmissivity (for normal incidence) of inhomogeneous lossless sea water droplets profiles.

by assuming constant T in the thin transition zones. Because the depth of the inhomogeneous zone is small, the downward radiation can be considered approximately the same as the upward radiation. The total radiation from the transition zone is therefore $T(1-\tau_h)+T(1-\tau_h)(1-E)\tau_h$. The sky radiation will be first attenuated by the transition zone, then reflected by the interface, and finally attenuated again by the transition zone. The combined reflected sky temperature is equal to $T_s(1-E)\tau_h^2$. It has been assumed that the refraction due to the thin transition zone is negligible. The resultant brightness temperature T_{BD} due to the presence of a lossy droplet transition zone is the sum of these three components; namely,

$$T_{BD}=T-(T-T_s)(1-E)\tau_h^2. \tag{21}$$

Note that the above expression does not include atmospheric absorption and atmospheric radiation, since the measuring radiometer is assumed by Nordberg *et al.* to be at low altitude ($\sim$130 m). Eq. (21) reduces to $T_B=ET+(1-E)T_s$ as it should if the transition zone is lossless.

To evaluate Eq. (21) for any zenith angles θ_1 without involving numerical integration, we shall simplify the calculations of both the sky temperature T_s and the transition zone transmissivity τ_h by making appropriate assumptions. The sky temperature T_s can be approximated as

$$T_s=T_m(1-\tau_a)+2.7\text{K}, \tag{22}$$

where 2.7K is the equivalent brightness temperature due to cosmic radiation, T_m is the mean effective temperature of the atmosphere and $\tau_a=e^{-\alpha\,\sec\theta_1}$, with α as the total attenuation factor for the atmospheric path in the zenith direction. The average zenith sky temperature T_s, observed under the experimental conditions of Nordberg *et al.* (1971), was about 20K and the corresponding attenuation factor α can be shown to be about 0.065, obtained by using an equivalent model atmosphere (fine weather with about 75% humidity). Thus, the sky temperature expressed as a function of the zenith angle is

$$T_s=268(1-e^{-0.065\,\sec\theta_1})+2.7\text{K}. \tag{23}$$

The transmissivity τ_h of the transition zone can be derived with the aid of the dielectric constant immediately above the air-sea interface, i.e., from

$$[\epsilon_0(v,0^+)]^{\frac{1}{2}}=[\epsilon_{0r}(v,0^+)-i\epsilon_{0i}(v,0^+)]^{\frac{1}{2}}$$

$$=[\epsilon_{0r}(v,0^+)]^{\frac{1}{2}}\left[1-i\frac{\epsilon_{0i}(v,0^+)}{2\epsilon_{0r}(v,0^+)}\right],$$

TABLE 2. Brightness temperature T_{BD} for horizontal polarization at nadir (droplets only): $T=282$K, $J=2$ or 3, $h=\lambda$.

v (m sec^{-1})	p (%)	$\epsilon_0(v,0^+)$	τ_h	T_{BD} (°K)	ΔT_{BD} (°K)
5	0.00	$1.000-i0.000$	1.000	129.1	5.9
10	0.05	$1.012-i0.018$	0.982	135.0	6.0
15	0.11	$1.025-i0.038$	0.963	141.0	6.0
20	0.17	$1.039-i0.059$	0.944	147.0	6.0
25	0.24	$1.054-i0.080$	0.924	153.0	6.0

if $\epsilon_{0i}(v,0^+)\ll\epsilon_{0r}(v,0^+)$. The transmissivity τ_h then is

$$\tau_h=\exp\left\{-\frac{4\pi}{\lambda\cos\theta_1}\int_0^h\frac{\epsilon_{0i}(v,0^+)}{2[\epsilon_{0r}(v,0^+)]^{\frac{1}{2}}}\cos^J\left(\frac{\pi}{2}\frac{z}{h}\right)dz\right\}$$

$$=\exp\left\{-\frac{4h\sec\theta_1}{\lambda(J+1)}\frac{\epsilon_{0i}(v,0^+)}{[\epsilon_{0r}(v,0^+)]^{\frac{1}{2}}}\right\}, \quad (24)$$

by assuming that the attenuation has a $\cos^J[(\pi/2)(z/h)]$ profile along the zone depth. For integer $J>1$, the profile will have a continuous first derivative at the air-droplets interface. With the combination of Eqs. (24), (23), (21), (15), (10) and (6), the apparent brightness temperature T_B of Eq. (21) can be conveniently evaluated for any zenith angles. Using the value of $\epsilon=23.41-i33.63$ at 19.35 GHz and choosing the values $C_1=10^{-4}$ and $C_2=6.5\times10^{-7}$, we find as shown in Table 2 that the calculated apparent brightness temperatures for horizontal polarization at nadir viewing can be made to agree with the curve-fitted rate of increase of 1.2C (m sec^{-1})$^{-1}$ with increasing wind speed according to Nordberg *et al.* (1971). For $J=2$ or 3 the results are virtually the same for the case $h=\lambda$.

The absolute values of calculated T_{BD} are about 11K higher than the measured values, indicating a possible calibration error of about 11K. The values of Table 2 are obtained on the assumption that the whole air-sea interface is covered with water droplets only and that there is no foam formation. Since the percent of foam-covered sea surface area increases with increasing wind speed, it appears that the present droplet model will be more realistic by taking the effect of foam formation into account. This will be done in the next section.

5. Combined effects of droplet and foam areas

For a partially foam-covered sea surface, Stogryn (1972) uses the simple concept that the total brightness temperature may be decomposed into

$$T_B=(1-F)T_{BD}+FT_{Bf}, \quad (25)$$

where T_{Bf} is the brightness temperature due to a 100% foam-covered surface, T_{BD} the brightness temperature due to a foam-free surface (and, in our application, that due to a droplet-covered surface), and F the fractional foam coverage which has been expressed as a function of wind speed W in the form (Stogryn, 1972)

$$F=7.75\times10^{-6}W^{3.231}. \quad (26)$$

Eq. (26), valid for $W<35$ m sec^{-1}, was obtained by a least-squares curve fit to several groups of experimental data (Murphy, 1968; Williams, 1970; Rooth and Williams, 1970; Monahan, 1969, 1971).

To express the brightness temperature T_{Bf} due to a 100% foam-covered surface as a function of both the frequency f and the nadir angle θ_1, the following available empirical form for horizontal polarization will be used:

$$T_{Bf}=(208+1.29f)(1-1.748\times10^{-3}\theta_1-7.336\times10^{-5}\theta_1^2+1.044\times10^{-7}\theta_1^3), \quad (27)$$

where f is the frequency (GHz), θ_1 the nadir angle (deg), and T_{Bf} the temperature (°K).

With the aid of (25)–(27), we can re-determine the constants C_1 and C_2 in the hope that the calculated brightness temperature T_B of Eq. (25) may have the desired rate of increase with increasing wind speed at the nadir viewing. It appears that by choosing $C_1=11\times10^{-3}$ and $C_2=-2\times10^{-6}$ the results shown in Table 3 are about the closest we can find without getting into the unreasonable situation that the percent droplet water content p decreases with increasing wind speed.

Note that the rate of brightness temperature increase is no longer constant with increasing wind speed. However, the increasing rate of ΔT_B in the last column of Table 3 may not be inconsistent with the experimental data of Nordberg *et al.* (1971). There are two possible explanations for the deviation. The first is that the rate of brightness temperature increase with increasing wind speed might not be constant but increasing, since an increasing rate of brightness temperature can be obtained by curve fitting to the data of Nordberg *et al.* (1971) if necessary. The second is that the fraction of foam area F of Eq. (26) might be too large at high wind speed as discussed by Williams (1970) and Blanchard (1971) since Eq. (26) was obtained by curve fitting without using the earlier analyzed results of Blanchard (1963) which show lower foam fractions at higher wind speeds. Thus, it appears that unless the measured rate of brightness temperature increase and/or the

TABLE 3. Brightness temperature T_B for horizontal polarization at nadir due to droplets and foam: $T=282$K, $J=2$ or 3, $h=\lambda$.

v (m sec^{-1})	p (%)	$\epsilon_0(v,0^+)$	τ_h	T_B (°K)	ΔT_B (°K)
5	0.00	$1.000-i0.000$	1.000	129.2	5.4
10	0.04	$1.009-i0.013$	0.987	134.6	6.4
15	0.07	$1.016-i0.024$	0.977	141.0	8.8
20	0.09	$1.020-i0.030$	0.970	149.8	12.8
25	0.10	$1.022-i0.034$	0.967	162.6	

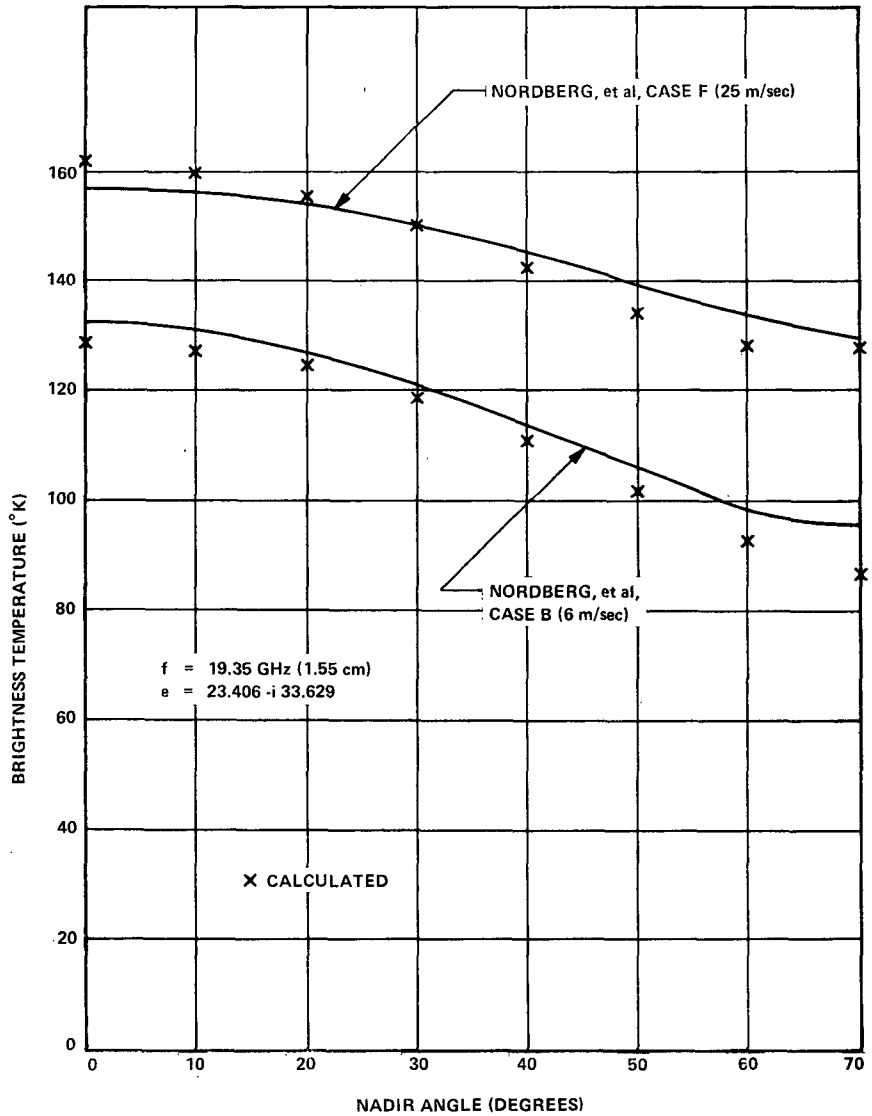

FIG. 9. Brightness temperature curves (modified theory).

increase of the fraction of foam area can be determined more accurately as a function of wind speed, the answer to the problem will remain unresolved.

The brightness temperature of the sea with droplet-covered and foam-covered areas at other nadir angles will now be calculated for $v=5$ m sec^{-1} $[\epsilon_0(v,0^+) = 1-i0]$ and $v=25$ m sec^{-1} $[\epsilon_0(v,0^+)=1.022-i0.034$ from Table 3] for comparison with observed data. The computed results are shown in Fig. 9. It is seen that the calculated points and the observed curve for $v=5$ m sec^{-1} agree fairly well with a vertical shift of about 3K which could be accounted for as experimental calibration error. For $v=25$ m sec^{-1} the calculated brightness temperature at nadir appears to be too high due to the too large ΔT_B increase shown in Table 3. At larger nadir angles the calculated brightness temperatures at $v=25$ m sec^{-1} appear to be too low. This could be attributed to the fact that at large wind speed and at large nadir angles the horizontal emissivity calculated from Shifrin's steepest-descent method is lower than that from Stogryn's numerical integration method as seen by comparison of Figs. 3 and 4. Thus, by using an appropriately reduced fractonal foam area factor F and Stogryn's emissivity, the calculated brightness temperatures at $v=25$ m sec^{-1} might not deviate too much from the measured data. In addition to the above-mentioned possible sources of discrepancy, the approximate sky temperature calculation shown in Eq. (23) might also introduce a few degrees Kelvin error at large nadir angles. The fact that the refraction effect in the inhomogeneous transition zone at oblique incidence has not been properly taken into account could also introduce errors, especially at large nadir angles. To include all these pos-

sible corrections properly, it is clear that a considerable additional amount of work is needed. Since the basic purpose of this paper is to introduce the absorbing-emitting concept of the droplet effect in the absorptive inhomogeneous transition zone, these corrections will not be included here.

6. Conclusions and discussion

Hollinger (1970, 1971) made measurements from a tower (20 m above sea surface) on a fixed ocean platform at 1.41, 8.36 and 19.34 GHz. Because of the effects of the tower structure on the brightness temperature measurements, he could not make reliable measurements between nadir and a nadir angle of about 20°. The absence of measurements at nadir makes it impossible to obtain the rate of brightness temperature increase at nadir with respect to wind speed. Any extrapolation of the nadir measurements from those made at angles of 20° or larger is speculative under the circumstances in addition to the fact that the effect of oblique incidence due to the presence of an absorptive inhomogeneous transition zone has not been investigated yet. It is evident that more measurements similar to those made by Nordberg *et al.* (1971) at 19.35 GHz are needed to establish the consistency of the measurements and to verify the validity of the modified theoretical model at other frequencies and for both polarizations. A critical test of the validity of the droplet model appears to be in showing that the volume fraction P of sea water droplets in the absorptive inhomogeneous transition zone immediately above the sea surface for a particular wind speed is insensitive to the frequencies used in measurement. Since no reliable nadir measurements of sea surface brightness temperatures at frequencies other than 19.35 GHz are available, there is an urgent need for such measurements for both polarizations.

It is also necessary to carry out experiments to determine the sea water droplet profile and its dielectric constant and attenuation characteristics in order to understand the fundamental nature of the transition zone at the sea-air interface. The determination of these parameters in the transition zone is not only required for brightness temperature measurements but also has important bearing upon the capacity of the sea surface to reflect and emit light and other electromagnetic radiation. In turn, these studies may have significant impact on the use of an air-sea boundary layer model in weather prediction. The meteorological phenomena occurring in the immediate neighborhood of the sea surface hold a key position among all the physical processes in the marine atmosphere, i.e., the layer defined as being controlled by the sea surface as a lower boundary. Recently, MacIntyre (1972) made a detailed study on the problem of jet formation and the origin of materials in the jet and film drops during bubble fractionation passage from sea to air. He examined a number of approaches in studying the flow patterns in breaking bubbles. He concluded that none of the approaches led to anything particular definitive about flow mechanisms in breaking bubbles.

From the results of computations, it is clear that the effect of absorptive sea water droplets in the inhomogeneous transition zone on the brightness temperature of the sea surface is important in that the transition zone first increases the air-sea interface brightness temperature and then attenuates and re-emits radiation to make significant contributions to the measured sea surface brightness temperature.

In passing, we mention that since the percentage of foam coverage on the sea surface as a function of wind speed is extremely difficult to determine from photographs, it would be ideal if we could obtain measurements at high wind speeds without encountering foam effects. This presumably could be done if the radiometer used in the measurements were of the narrow-beam type. The data obtained by narrow-beam radiometers could then can be grouped so as to discard foam-contaminated data. The data from pure droplet-covered areas could then be analyzed by the approach outlined in Section 4 without using the uncertain foam coverage factor F.

After the completion of this study two papers (Wagner and Lynch, 1971; Wu and Fung, 1972) directly related to microwave sea brightness temperatures came to my attention. It is therefore appropriate at this point to present some general reflections on this complex problem. After about a decade of theoretical and experimental studies from divergent views by various investigators, it seems that the opportune time has come for us to make the transition from piecewise analyses to a synthesis. The factors that influence microwave sea brightness temperatures appear to be many. For completeness we shall discuss briefly factors other than the air-sea interface region presented in this paper. Two other major factors are the shadowing and multiple-scatter effects analyzed by Wagner and Lynch (1971) and the capillary wave effects analyzed by Wu and Fung (1972).

Using one-dimensional geometric optics, Wagner and Lynch developed a cylindrical rough-surface emission and scattering model that accounts for surface shadowing effects and contributions from double-scattered radiation. Their results, including estimated effects of both foam and sea spray, appear to be in excellent agreement ($\sim$1K) with at least one case of the observations made by Nordberg *et al.* (1971). The limitations of the model are that the one-dimensional surface roughness model (i) assumes cylindrical symmetry and thus prevents the mixing of two Fresnel polarization components, and (ii) ignores the effects of actual sea surface slope distribution anisotropy due to up-and-down wind and cross-and-parallel wind. Although the model has its limitations, it is important

to recognize that the effects of shadowing and double-scatter can be quite significant at large oblique observation angles, especially at high wind speed.

The composite-scale rough-surface emission and scattering model, analyzed by Wu and Fung, according to a noncoherent scattering theory of the type described by Semyonov (1966), accounts for (i) the effect of small irregularities of capillary waves on the scattering characteristics of large undulations of gravity waves by modifying the Fresnel reflection coefficients, and (ii) the effect of large undulations on small irregularities by averaging the scattering cross sections of small irregularities over the surface normals of the large undulations. Comparison of the results of the composite-surface model with Hollinger's experimental results at 8.36 GHz indicates a significantly improved agreement over that shown by Stogryn's single-surface model, and a sensitivity to wind speed at nadir. The validity of the model could have been more convincing if the comparison between Hollinger's measurement results at 1.41 and 19.34 GHz and their corresponding theoretical results were also shown. It is suspected that no efforts were made to compare the model results with the observations of Nordberg *et al.* (1971) because the observed results included foam effects. The model assumption that the sea has an isotropically rough surface ignores the actual slope distribution anisotropy due to up- and cross-winds which were considered in Stogryn's single-surface model. The use of stationary phase method in the model probably also introduces some gross approximations.

It is important to note that the sensitivity of the composite-surface model to wind speed at nadir results from the modified Fresnel coefficients due to the presence of capillary wave irregularities on large gravity waves. The dominating assumption of the absorptive inhomogeneous transition zone of the model presented in this paper is that the index of refraction of the air-sea interface region is a function of both the wind speed and zone height. The sensitivity of zone index of refraction to wind speed is translated directly to corresponding variations in Fresnel coefficients. It is in this aspect that the composite-surface model and the present air-sea interface model have a common ground. Whether the droplet effect or the capillary wave, rough-surface effect is dominant is a question to be resolved. By synthesizing all apparently possible views it appears that a complete model should include the effects of the atmosphere, foam, air-sea interface droplets, capillary waves superimposed on gravity waves, and shadowing and multiple-scatter. If reliable low-flying radiometer data can be selected as foam-free, the data may be used without considering the effects of the atmosphere and foam. If only measurements at nadir are to be compared, the effect of shadowing and multiple-scatter can be neglected. Theoretically, the present inhomogeneous droplet model could include all the above-mentioned effects, but combining all these effects into a form convenient for computational purpose is not a trivial task. The reason that the present droplet model uses Shifrin's results instead of Stogryn's results is that the latter requires a prohibitive amount of numerical integration to determine the appropriate constants C_2 and C_3 of Eq. (15). Shifrin's results are already in a computationally compact form suitable for our purposes. Accordingly, any future unified complete model should be cast in a form suitable for convenient and efficient computation of C_2 and C_3.

Acknowledgments. The author wishes to thank A. Stogryn for supplying the computed data shown in Fig. 3, many stimulating discussions, and critical reading of the manuscript.

REFERENCES

Blanchard, D. C., 1963: The electrification of the atmosphere by particles from bubbles in the sea. *Progress of Oceanography*, Vol. 1, M. Sears, Ed., MacMillan, 73–197.

——, 1971: Whitecaps at sea. *J. Atmos. Sci.*, **27**, 645.

——, and A. H. Woodcock, 1957: Bubble formation and modification in the sea and its meteorological significance. *Tellus*, **9**, 145–158.

Cox, C., and W. Munk, 1954: Measurements of the roughness of the sea surface from photographs of the sun's glitter. *J. Opt. Soc. Amer.*, **44**, 838–850.

Hollinger, J. P., 1970: Passive microwave measurements of the sea surface. *J. Geophys. Res.*, **75**, 5209–5213.

——, 1971: Passive microwave measurements of sea surface roughness. *IEEE Trans. Geosci. Electron.*, **9**, 165–169.

MacIntyre, F., 1972: Flow pattern in breaking bubbles. *J. Geophys. Res.*, **77**, 5211–5228.

Mandelbaum, H., 1956: Evidence for a critical wind velocity for air-sea boundary process. *Trans. Amer. Geophys. Union*, **37**, 685–690.

Monahan, E. C., 1969: Fresh water whitecaps. *J. Atmos. Sci.*, **26**, 1026–1029.

——, 1971: Ocean whitecaps. *J. Phys. Oceanogr.*, **1**, 139–144.

Munk, W. H., 1947: A critical wind speed for air-sea boundary processes. *J. Marine Res.*, **6**, 203–218.

——, 1950: Origin and generation of waves. *Proc. First Conf. Coastal Engineering*, Long Beach, Calif., Council on Wave Research, The Engineering Foundation, 1–4.

Murphy, H., 1968: Percentage foam vs wind velocity. Internal report, University of Miami, Coral Gables.

Nordberg, W., J. Conaway and P. Thaddeus, 1969: Microwave observations of sea state from aircraft. *Quart. J. Roy. Meteor. Soc.*, **95**, 408–413.

——, ——, D. B. Ross and T. Wilheit, 1971: Measurements of microwave emission from a foam-covered wind-driven sea. *J. Atmos. Sci.*, **28**, 429–435.

Roll, H. V., 1965: *Physics of the Marine Atmosphere*. New York, Academic Press, p. 24.

Rooth, C., and G. Williams, 1970: Microwave radiometry of the ocean. Quarterly report, University of Miami, Coral Gables.

Semyonov, B., 1966: Approximate computation of scattering electromagnetic waves by rough surface contours. *Radio Eng. Electron. Phys.*, **11**, 1179–1187.

Shifrin, K. S., and S. N. Ionina, 1968: Thermal radiation and reflection from a rough sea surface in the microwave region. *Tr. Gl. Geofiz. Observa.*, No. 222.

Stogryn, A., 1967: The apparent temperature of the sea at microwave frequencies. *IEEE Trans. Antennas Propagat.*, **15**, 278–286.

——, 1971: Equations for calculating the dielectric constant of saline water. *IEEE Trans. Microwave Theory Tech.*, **19**, 733–736.

——, 1972: The emissivity of sea foam at microwave frequencies. *J. Geophys. Res.*, **77**, 1658–1666.

——, 1972: A study of radiometric emission from a rough sea surface. NASA Contract Report CR-2088.

Tang, C. C. H., 1974: Multiple scattering from finite inhomogeneous media. *J. Appl. Phys.*, **45**, 1115–1126.

Wagner, R. J., and P. J. Lynch, 1971: Sea brightness temperatures at microwave frequencies. *Proc. AGARD Conf. Propagation Limitations in Remote Sensing*, No. 90, Colorado Springs.

Williams, G. F., 1970: Comments on "Fresh water whitecaps." *J. Atmos. Sci.*, **27**, 1220.

Wu, S. T., and A. K. Fung, 1972: A noncoherent model for microwave emissions and backscattering from the sea surface. *J. Geophys. Res.*, **77**, 5917–5929.